A Novel Quadruple Active Bridge DC Converter With Reduced Inductor Current for EV Battery Charging

Anil Kumar BOYA , *Batchalakura JYOTHI*

Department of Electrical and Electronics Engineering, Koneru Lakshmaiah Education Foundation
Vaddeswaram, Guntur, 522302 Andhra Pradesh, India

anilkumarvalmiki4302@gmail.com, jyothieee@kluniversity.in

Abstract. *A bidirectional DC-DC converter can diminish the uncertainty of PV generation and enhance system reliability when integrated with energy storage systems. Usually, a Dual Active Bridge (DAB) converter with soft switching capability essentially matches the needs of an energy storage system. The DAB not able to reduce the inductor current stress when load is increased, and thus, the efficiency is decreased. To address this issue, we present a novel Quadruple Active Bridge (QAB) converter. In terms of enhancing the efficiency along with mitigating the current stress on the Low Voltage (LV) side, the LLC resonant converter with a constant pulse width modulation scheme was implemented. Finally, the QAB-LLC converter fed with Electric Vehicle's (EV's) Battery has been verified in MATLAB/Simulink and it results in a maximum State of Charge (SOC) and, maximum voltage capability which provides a high efficiency along with minimum inductor current stress on LV side.*

Keywords

Constant Current Constant Voltage (CC-CV), Dual Active Bridge, Electric Vehicles, lithium ion, Photovoltaic, Quadruple Active Bridge.

1. Introduction

To protect inhabitants from the environmental pollution, India's major cities are adopting electric transportation not only to saves money but al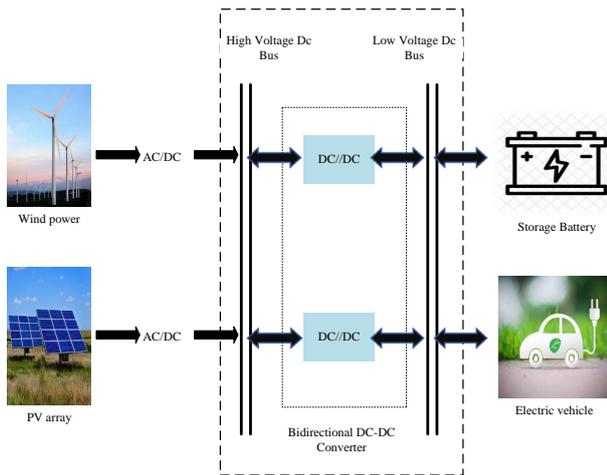so the environment [1]. Currently, the number of Electric Vehicle's (EV) users are increasing in India. The most important factor for increasing, the number of EV's is zero-greenhouse gas emissions [2]. The main issue regarding EVs is the lack of charging stations. Depending on different EV type, charging levels are presented in Level 1, and Level 2. The EV is dependent on battery capacity for the whole charge, which takes 16–20 hours at Level 1 rated at 120 V. Level 2 is at 240 V single phase home charging station that ensures a fully charged battery in 8 hours with overnight charging. These two levels include Electric Vehicle Supply Equipment (EVSE) to converter AC power to DC for charging the car. Level 3 is at 480 V DC fast charging station that delivers power directly to the battery within an hour.

Like petrol stations, it can be built on highways and city filling sites. To convert AC to DC, it uses a three-phase power supply with 480 V or more.

Global warming occurred during the early stages of the industrial revolution due to the use of fossil fuels. To reduce this impact, the energy produced by wind power, solar Photovoltaic (PV), and hydroelectric power will help in decreasing CO_2 emissions. By the usage of Renewable energy sources, a significant impact on the grid is observed. This problem can be avoided by using a bidirectional DC-DC converter to connect an energy storage device to the DC-link as shown in Fig. 1.

In a bidirectional DC-DC converter, the transformer determines the load voltage rating, with DC-link voltage based on the transformer turns ratio, as shown in Fig. 2.
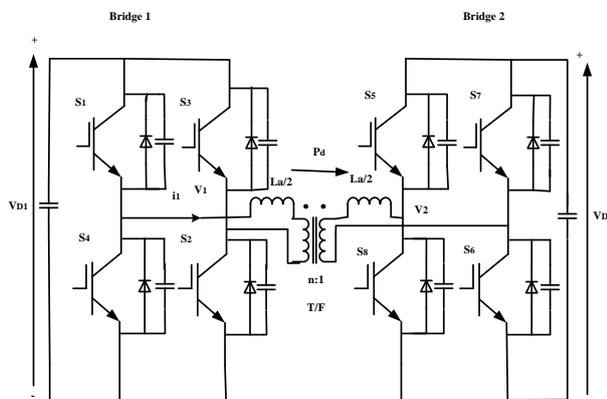
Fig. 1: Bidirectional DC-DC converter.

Fig. 2: Pictorial representation of bidirectional DC-DC converter.

In [3], a pre-charging circuit is employed to reduce a large amount of inductor current stress at the start of the system to the two unequal voltages. The zero-voltage switching is usually provided by LC circuit. The energy loss takes place by turning on the switch. The switch instantly turns on through zero supply voltage by providing milliseconds with delaying the gate voltage. Large voltage spikes can be mitigated in traditional full-bridge DC-DC converters by using high-rated diodes but it leads to very low reverse recovery characteristics are observed practically.

A circuit was presented to address the snubber requirement, but it was found that the implementation of this circuit resulted in a decrease in efficiency. In [4], a small fraction amount of enhancement is applied to enhance the efficiency of the active clamp circuit, which, in turn, results in a large current stress. To mitigate the current stress in high voltage applications two auxiliary inductors are connected in series with two MOSFETs [5]. The author in [6] presents a large voltage spike due to delay time in turn-on time for charging the snubber capacitor with the inductive current. The operation mode of an LLC converter

depends on its voltage gain. Adding an extra inductor increases the cost and size of the converter, making it more suitable for high voltage applications rather than Low Voltage (LV) applications [7]. The main disadvantage is that the voltage gain limits the switching frequency variation. The mode of operation is determined based on the constant amplitude and pulse width, which allows for operating the converter without limiting the voltage gain. The chosen mode of operation can then determine the voltage gain [8].

The optimization design is critical by connecting the EV battery to the LLC converter as suggested in [9]. In [10] presents a solution using interleaved LLC resonant converter and cascaded voltage-doubler circuits for efficient charging of deeply depleted plug-in electric vehicle batteries. It successfully tackles the issue of extending the converter's operating range by mitigating the impact of transformer parasitic capacitors. The SOC and charging current of the battery define the converter's output voltage. To charge the deeply depleted battery, a voltage double-circuit was used with a large voltage gain to minimize the parasitic capacitor negative effect. To improve efficiency at low load, LLC converters can work in different regions like frequency-modulated full bridges, two-phase and single-phase half-bridge [11]. Higher power density is achieved with a resonance inductor placed in a transformer. The literature outcomes of bidirectional DC-DC converters suffer from various critical issues like complex design approaches for various output voltage ranges and difficulty to generate bidirectional. As a result, the Dual Active Bridge (DAB) bidirectional DC-DC converter was proposed, which includes high power density, high current density, voltage variations, and two bridges on the source and load sides [12] as shown in Fig. 3.
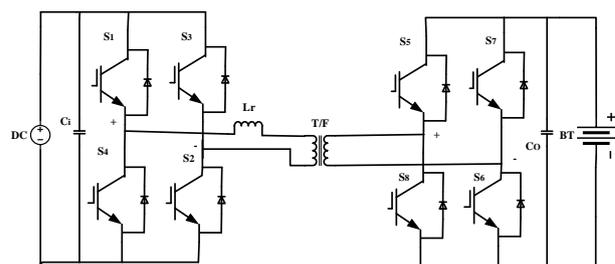

Fig. 3: DAB converter.

It generates square wave voltage at the primary and secondary sides and determines the inductor current stress of the device by supplying a constant Pulse Width Modulation (PWM) signal [12] and [13]. The main drawback is high turn-off power loss when it operates voltage gain greater than unity. By introducing a Zero Voltage Sequence (ZVS) applied to bridges by changing of phase shift. Considerable modulation techniques are Phase Shift Modulation (PSM) and

Triangular Current Modulation (TCM) or Trapezoidal Current Mode (TCM).

DAB activates the reverse power flow, then bidirectional is easily achieved. A converter always depends on input and output voltage, input power, design parameters, and voltage gain. Maintaining a low duty cycle ratio and minimizing leakage inductance are crucial factors in achieving ZVS for all switches and improving efficiency. The three-level DAB converter generates four square waves with varying amplitudes for a wide range of voltage gain [14]. In [15] medium-voltage DAB converter presents a compact solution for EV charging stations, eliminating the need for a bulky MV-LV transformer, enabling efficient and high-power fast charging. However, a potential challenge lies in the complexity and cost associated with integrating and controlling this high-power converter topology. To decrease the current stress and eliminate the reactive power, a DAB–SRC (Series Resonant Converter) is employed by four degrees of freedom under different battery voltages [16]. The DAB converter is controlled by the single-phase shift control [17] extended phase shift control [18], dual-phase shift, and triple-phase shift ratio [19] which increases the efficiency depending on the phase shift ratio. Introducing variable phase shifts improves the performance of soft switching and DAB as demonstrated in [20]. Setting the switching frequency to the resonance frequency and maintaining unity gain enables achieving high efficiency in onboard chargers [21]. The summary of the operating performance conditions of the above-mentioned topologies is presented in Tab. 1.

In [22] DAB consists of four full bridges, first one can control the PV source, second one connected to a stationary storage system and can function as either a source or a load, and the remaining two to control the charging of the battery units for up to two cars. To create a magnetic node and connect more than two ports, all ports are connected through a high-frequency multi-winding transformer. This is helps in the era of multiple and different voltages are involved where a bidirectional power flow is required, such as in smart grids.

To effectively identify the defective components and prevent the system from collapsing, an Open-Circuit Fault (OCF) diagnosis technique is provided for DAB converters operating under advanced Triple Phase Shift (TPS) management based on the resonant phenomenon under fault situations [23].

Households in foreign countries are progressively purchasing at least two EV's necessitating the usage of energy storage devices and bridge converters like DAB converters. Due to the growing number of EV's on the road, converter, and component demand is rising. Connecting various energy storage devices to a single DC bus serves is one solution. The operation of bidirectional DC/DC converters like DAB and QAB depends on power transfer and voltage. AQAB, SQAB-V (Symmetric Quadruple Active Bridge - Voltage), and SQAB-P (Symmetric Quadruple Active Bridge - Power) are some examples of QAB converters. In comparison to these converters, the AQAB converter is more efficient and uses fewer modules, although it currently has an issue with the balance of the bridges depending on the turn's ratio [24]. In [25] HESS, or two integrated storage components like batteries and ultracapacitors, have been used to construct a QAB for EVs. These components are driven by the driving train and the charging port. In storage components of the system QAB can be used in a Vehicle to Grid (V2G) scenario since power can be exchanged between all the ports.

Reference [26] discusses the integration of Distributed Energy Resources (DER) and Distributed Energy Storage systems (DESS) into the grid. A Modular Multilevel Converter (MMC)-based Solid-State Transformer (SST) uses a SST and a QAB converter as its primary parts to accomplish this integration. Each QAB converter links to two MMC cells, and its third port allows for connections with either a DER or DESS. The fourth port of each DC/DC converter must be connected to the LVDC bus that could interact with a Low Voltage AC (LVAC) grid by way of a power inverter. By integrating DER and DESS while maintaining the same power transfer in the MMC cells, this keeps the voltages in the capacitors of the MMC cells balanced.

In each of the QAB's medium-frequency transformers have a balancing winding that is an additional winding. The transformers' balancing windings are paralleled to allow a current to circulate among the three phase transformers, reducing the unbalance in the clusters connected by deltas [27]. Consequently, the amount of zero sequence current necessary to balance the cluster powers for a particular degree of unbalance is similarly decreased. By doing this, the overall current running through the CHB's devices is decreased, as is the over-current rating needed to handle a specific unbalance. A current balancing coupling inductor for power transmission and zero voltage switching that does not need an additional magnetic volume is used in an asymmetric QAB converter [28] dependent on the turns ratio to maintain current balance. A setup with an MAB converter [29] utilizing a stiff voltage source on the transformer's magnetizing inductance results in naturally decoupled power flows. As a result, the configuration displaces the requirement for a high-performance dynamic decoupling controller and permits independent power flow control tuning

Tab. 1: Comparison of isolated DC-DC converter specifications.

Topology	Reference	Structure	Power (kW)	Output voltage (V)	No. of switches/diodes	Modulation method	Major advantages/disadvantages
Resonant converter	9	LLC full bridge	3.3	250–450	4/4	Pulse frequency	ZVS has a broad range and can adjust output voltage during low load, high efficiency, compact size, and low EMI. Bidirectionality is not normally obtained. The switching frequency is equal to the resonant frequency, and the modeling approach to producing a greater output voltage range is complicated.
	10	Interleaved CLLC + cascaded voltage double rectifiers	1.5	50–420	4/4	Pulse frequency	
	11	Hybrid LLC	3.2	250–400	4/4	Pulse frequency	
DAB converter	13	Conventional DAB	20	200–450	8/0	Single + dual + triple phase shift	Bidirectionality, implicit soft switching, voltage output transfer ratio. For Single Phase Shift (SPS), securing ZVS at low loads is hard.
	14	Three-level DAB + blocking capacitor	3.5	200–700	16/8	Single phase shift	
	15	MV DAB	12	520–820	8/0	Single phase shift	
	16	DAB-SRC	4.5	200	8/0	Phase shift	

of the remaining ports. The proposed arrangement ensures that the HF transformer is appropriately designed to ensure a low leakage inductance in one port (master) without the addition of an external inductor and a comparably higher leakage inductance in the remaining ports (slave).

The authors in [30] lists the two primary architectures for these converters. Based on isolation and control strategies, Architecture-I uses unique two-port DC-DC converters to connect each source to the DC bus and based on source connection methods and port numbers, Architecture-II utilizes a single multiport converter to link all sources to the DC bus.

The operation, number of components, benefits and drawbacks, cost and efficiency of the medium voltage and medium frequency power converters are examined with respect to various SST topologies, configurations, power and voltage ratings, advantages, and related applications. Further, it is described how various SST topologies are implemented in the fields of solar PV, wind power conversion and transmission, traction, smart grid, MG, and DC charge stations [31].

The proposed QAB converter develops a high efficiency in EV battery applications by using of LLC converter.

The novelty of the proposed QAB converter is as follows:

- Reducing the inductor current stress by the appropriate LLC circuit configuration design in QAB.

- Increasing the efficiency of an EV's battery with respect to the DC link voltage.

2. Quadruple Active Bridge Converter

The Quadruple Active Bridge (QAB) converter carried out by using four bridges are indicated as V_a, V_b, V_c, V_d out of which three bridges are used for Medium Voltage (MV) side (b, c, d) and one on the LV side (a) is depicted in Fig. 4 [32]. The power of QAB is easily computed using the MV and LV cells [33] in Eq. (1), Eq. (2) and QAB is cost-effective because it requires a smaller number of modules along with single high-frequency transformer [34]. The transformer ratio, n of the QAB converter is defined as a number of modules of the MV side w.r.t the LV side given in Eq. (3).

$$P_{MvCell} = \frac{P_{QAB}}{N_{MvCell}}, \tag{1}$$

$$P_{LvCell} = \frac{P_{QAB}}{N_{LvCell}}, \tag{2}$$

$$n = \frac{N_{MvCell}}{N_{LvCell}}. \tag{3}$$
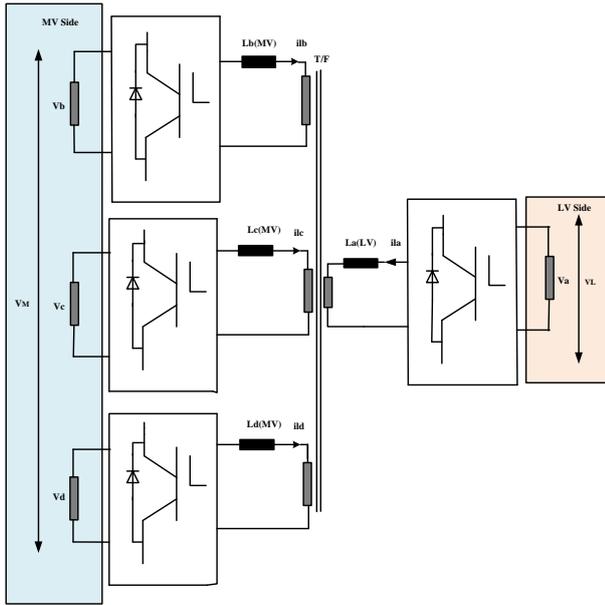
Fig. 4: QAB converter.

Fig. 5: One bridge on MV cell.

For a simple analysis of the converter, the voltage across the MV and LV sides is changed by rectangle voltage sources (V_a, V_b, V_c, V_d) based on switching actions. For example, let us consider one bridge on an MV cell with an R load. It has four switches as shown in Fig. 5.

The switch S1 and S2 are turned on and S3 and S4 are turned off, it generates positive voltage. Similarly, S1 and S2 are turned off and S3 and S4 are turned on which generates a negative voltage. Based on this analysis, it generates rectangular voltage sources, and an equivalent circuit has presented in Fig. 6.

The current slope of inductor on MV (L_b, L_c, L_d), LV side (L_a) and the voltage on the center point v_x is given by Eq. (4) and Eq. (5).

$$\frac{di_{Li}}{dt} = \frac{v_i - v_x}{L}, \tag{4}$$

$$v_x = \frac{v_a + v_b + v_c + v_d}{4}, \tag{5}$$

where i_{Li} is the inductor current on MV and LV bridges.

By using this Phase Shift Modulation (PSM), the input rectangle voltages V_a, V_b, V_c, V_d with constant frequency to the transformer for controlling power at phase shift (ψb) [33].

Any converter depends on input, output voltage, and load. The MV rectifier is controlled by the input voltage of the QAB converter and then produces the load voltage. Only power exchange in the MV and LV sides under balanced conditions is possible with
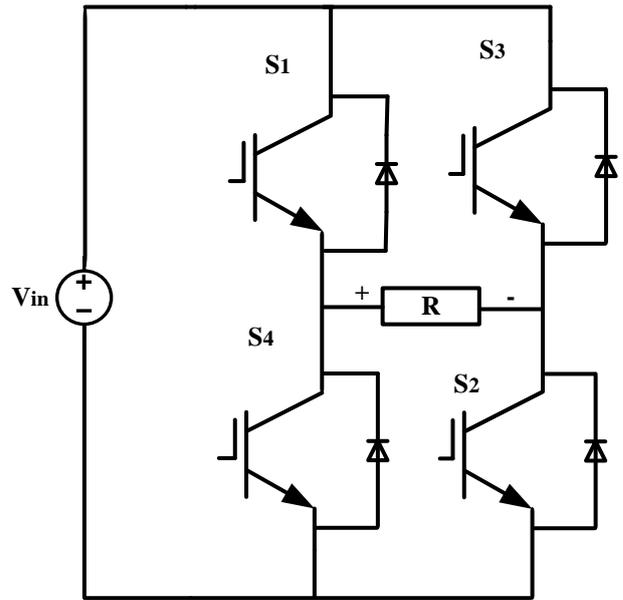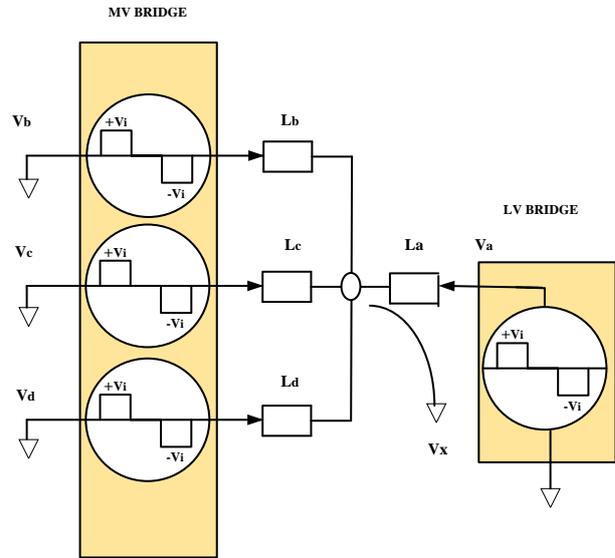

Fig. 6: Equivalent circuit of QAB converter.

a smaller phase shift angle followed by Eq. (6):

$$P = \frac{v_M v_L \psi_b (1 - \psi_b)}{2\pi f_s L_{equ} n}, \tag{6}$$

where v_M, v_L is the MV and LV DC link, f_s is switching frequency and ψ_b is the phase shift.

Usually, L_{equ} is termed as equivalent inductance on the LV side and it can be determined using the LV and MV inductances given by Eq. (7):

$$L_{equ} = L_a + \frac{L_b + L_c + L_d}{3n^2}, \tag{7}$$

The power transfer depends only on the leakage inductance, changing of duty ratio, turns ratio, phase

shift with constant input and output voltage along with switching frequency. When the phase angle is high, more reactive power is attained. Particularly, the PSM occurs is when there is a fault occurring in any one of the QAB cells, then the remaining cells will operate. But this PSM, operates the QAB converter in a hard switching manner under faulty conditions. QAB converter operates in the symmetric mode because of the low RMS value current present at leakage inductance by applying Triangular Current Modulation (TCM). The power flow control among the bridges and reactive current is reduced by the duty cycle in TCM [34]. Under the balanced conditions the duty cycle on LV is D1 and MV side bridges are of the same i.e., D2=D3=D4. The TCM's main principle is to apply a triangle current on inductors and achieve voltage across the winding V_a and V_b with phase shift ψ has shown in Fig. 7 as a result, v_x is calculated using the Eq. (8).
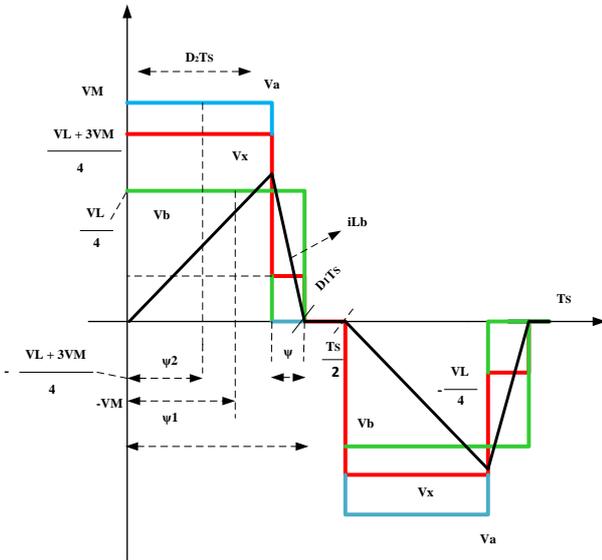

Fig. 7: Main waveforms of QAB convert.

$$v_x = \begin{cases} \dfrac{nv_L + 3v_M}{4}, & 0 < t < d_2T_s, \\ \dfrac{nv_L}{4}, & d_2T_s < t < d_1T_s, \\ 0, & d_1T_s < t < \dfrac{T_s}{2}. \end{cases} \quad (8)$$

During the time interval between $0 < t < d_2T_s$, the inductor current begins at zero and rises to its higher value iL_b. Similarly, during the $d_1T_s < t < \frac{T_s}{2}$ period, the currents decline from iL_b to zero.

During the $0 < t < d_2T_s$, the current variation in the inductor can be calculated from Eq. (4) and Eq. (8).

$$\Delta i_{b(0<t<d_2T_s)} = \frac{D_2(v_M - nV_L)}{4Lf_s}. \quad (9)$$

Similarly, for period $d_2T_s < t < d_1T_s$ and $d_1T_s < t < \frac{T_s}{2}$, the change in inductor current is obtained as follows:

$$\Delta i_{b\left(d_2T_s<t<\frac{T_s}{2}\right)} = \frac{(D_2 - D_1)(nV_L)}{4Lf_s}. \quad (10)$$

To achieve Zero Current Switching (ZCS), the condition for inductor currents between switches is determined based on Eq. (9) and Eq. (10). The relationship between D_1 and D_2 is then described.

$$\Delta i_{b(0<t<d_2T_s)} = \Delta i_{b\left(d_2T_s<t<\frac{T_s}{2}\right)}. \quad (11)$$

$$D_2 = \frac{D_1(nV_L)}{v_M}. \quad (12)$$

The input DC bridges' transmitted power can be calculated as:

$$P_i = V_iI_i, \quad (13)$$

where, P_i = input power, V_i = input voltage at MV side DC link = v_M, I_i = input current at MV DC bridges, v_L = LV DC link.

Let us consider the average current on the cell 'b' at MV side is calculated as:

$$I_b = \frac{2}{T_s} \int_0^{D_2Ts} i_b(dt), \quad (14)$$

where, $i_b = \frac{D_2(v_M - nv_L)}{4f_sL}$, $0 < t < d_2T_s$ from Eq. (10) it gives:

$$I_b = \frac{D_2^2(v_M - nv_L)}{4f_sL}, \quad (15)$$

The power calculated on the cell 'a' of LV side bridge is written as:

$$P_a = v_MI_b, \quad (16)$$

$$P_a = \frac{D_1^2(v_M - nv_L)(nv_L)^2}{4f_sLv_M}. \quad (17)$$

Similarly, the power cell 'b' of MV side bridge:

$$P_b = \frac{3D_1^2(v_M - nv_L)(nv_L)^2}{4f_sLv_M}. \quad (18)$$

TCM will operate the QAB converter in a soft switching manner under faulty conditions. With different duty ratios on the MV cells, it gives different power levels i.e., more amount of power observed one after another on MV cell. Large inductor current stress on the LV side is a major issue with the QAB converter. To overcome this, two or more bridges are connected in parallel by applying a fixed switching frequency with a 50 % duty cycle, However, it increases the complexity of the system [33]. As a result, an LLC resonant converter is proposed in QAB.

Figure 8 represents a visual depiction of QAB and DAB comparison, which shows why QAB has been preferred in DC applications over DAB.
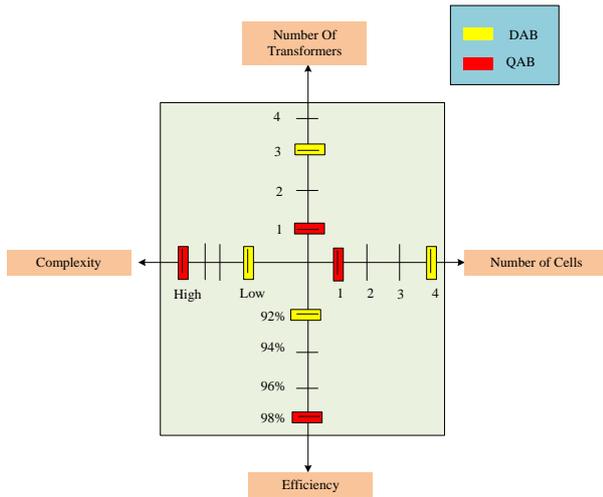
Fig. 8: QAB and DAB performance parameters are compared qualitatively.

3. Battery With DC Motor Bidirectional DC-DC Converter

High voltage applications like EV charging station usually consists of SST. SST consists of three stages i.e., MV stage (AC to DC), Medium Frequency (MF) converter, LV stage (DC to AC) [35]. The MF converter, also known as a DC-DC converter, which is used for power exchange between two stages stated above. The DC-DC converter supplies power to the EV battery, resulting in reduced current stress, stable voltage levels, and adjusted torques according to motor specifications [36], as illustrated in Fig. 9. The driving range of the battery imposes limitations on the performance of the EV battery and motor during motoring and regeneration modes. This configuration improves the converter's efficiency and establishes a connection to the main DC-DC converter, specifically the QAB converter of the charging station. In EV applications, DC-link of a battery is coupled to a bidirectional DC-DC converter.
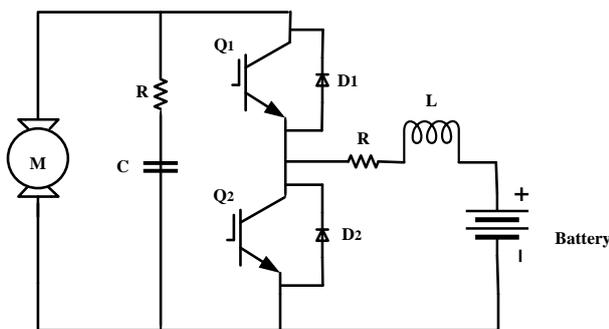

Fig. 9: Battery with Dc Motor Bidirectional DC-DC Converter.

The bidirectional DC-DC converter performs boost operation beside lower switch Q2 and upper anti parallel diode D1 and in buck operation with upper switch Q1, lower anti parallel diode D2 [35] as shown in Fig. 9.

Battery-fed EV present a High Voltage (HV) battery Lithium ion (Li-ion) are of 250 to 430 V. Most of the EV batteries are Li-ion batteries which are rechargeable and long charge/discharge cycle high energy density or high energy per unit mass, the weight of the vehicle is minimal [36]. By increasing the battery lifespan with bidirectional DC-DC converter it will be implemented by Constant Current Constant Voltage (CC-CV) algorithm. CC is used first step till the battery attains its normal voltage. After that, a Constant Voltage (CV) step is used to gradually reduce the charging current until the SOC reaches 100 % as shown in Fig. 10.
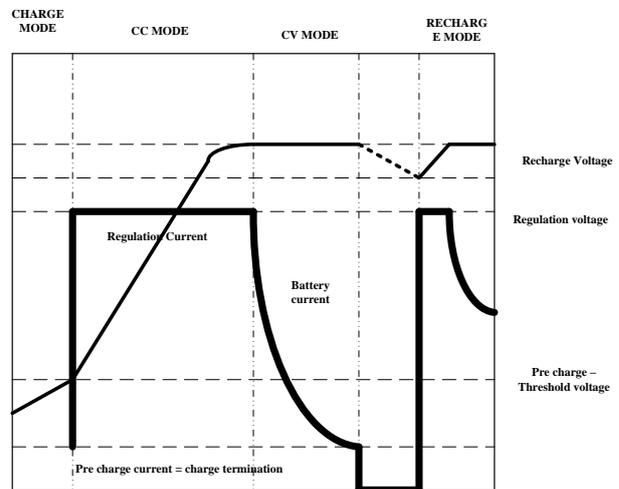

Fig. 10: Battery charge operation modes.

A detailed explanation of battery control strategy with CC-CV algorithm has presented in section VI. The process of continuous Constant Current (CC) charging is like pumping air into balloon continuously until it blows out. For this purpose, the battery SOC will charge up to 80 %, after the CC charging process CV will apply to decrease the current progressively when SOC attains 100 %.

4. Proposed Quadruple Active Bridge Design

In the proposed DC-DC converter architecture, QAB structure is used which has three modules [34]. Selecting the number of modules in QAB architecture, it increases the efficiency with less energy storage systems as compared to DAB converter. The proposed architecture supplies the DC-link voltage symmetrically. When the voltage gain is unity, the DAB converter

has the advantage of soft switching operation. If it is greater than a unity the DAB converter has large amount of leakage inductor current stress. To overcome this issue, in [12] simply presenting a DAB-SRC which further increase the efficiency. However, with increases in the loads, the DAB converter will not be able to meet the specific requirements like reducing the high-frequency transformer design. By choosing the number of modules and creating a bidirectional DC-DC converter with switching frequency, phase angle, duty cycle, leakage inductance, QAB converters are selected to overcome the drawbacks of DAB.

Section 4.1. elaborates on the design of a QAB-LLC converter for EV battery chargers. The 480 V QAB LLC converter is designed to charge a 27.9070 Ah of 430 V battery.

4.1. Design of QAB Converter

The design procedure of the proposed QAB converter considers the specifications presented in Tab. 2.

Tab. 2: QAB converter specification.

Rated Power (P)	MV DC link ($V_{MV\,DC}$)	LV DC link ($v_{LV\,DC}$)	Switching frequency (f_s)	n
1 MW	480 V	430 V	20 kHz	3

$$F_r = \frac{1}{2\pi}\sqrt{L_r C_r}. \tag{19}$$

The resonant capacitor is estimated as:

$$C_r = \frac{1}{4\pi^2 f_r^2 L_r}. \tag{20}$$

$$C_r = \frac{1}{4 \cdot \pi^2 \cdot 20^2 \cdot 10^6 \cdot 42.36 \cdot 10^{-6}} = 1.5\,\mu\text{F}. \tag{21}$$

The main drawback of QAB converter is large amount of current stress on LV side in order to reduce this effect additional resonant inductor should be added on LV side. The value of L_r is selected depending on transformer construction i.e., if the transformer turns is of different in MV with respect to LV side than it will affect the inductor current stress on LV side. Without affecting the transformer turns ratio an external resonant inductor added which is equal to the resonant inductor.

On MV side, the ZVS is attained by the resonant frequency equal to switching frequency. On LV side the C_r and L_r will affect the soft switching. Soft switching is easy with larger resonant current by considering the dead time. The resonant inductor would be used to attain the ZVS at any load condition:

$$L_r = \frac{\gamma A_v t_{dead}}{2 f_s c_i}, \tag{22}$$

where, A_v is the voltage gain, t_{dead} is the dead time, f_s - switching frequency, c_i is the input capacitor, γ is the is the output voltage control variable. The value of A_v calculated depending on the DC link voltage (V_{DC}), battery voltage V_b and turns ratio is given as:

$$A_v = n\left[\frac{V_b}{V_{DC}}\right]. \tag{23}$$

Battery-fed Electric Vehicles (EVs) commonly utilize the QAB converter with Li-ion batteries. When three QAB converter modules are connected to an MV DC link, each module operates at 160 V as the initial voltage. However, an adjustment of 480 V is applied to the connected modules. The battery voltage is between 230 V to 430 V. The input – output relation and corresponding gain range is shown in Fig. 11.
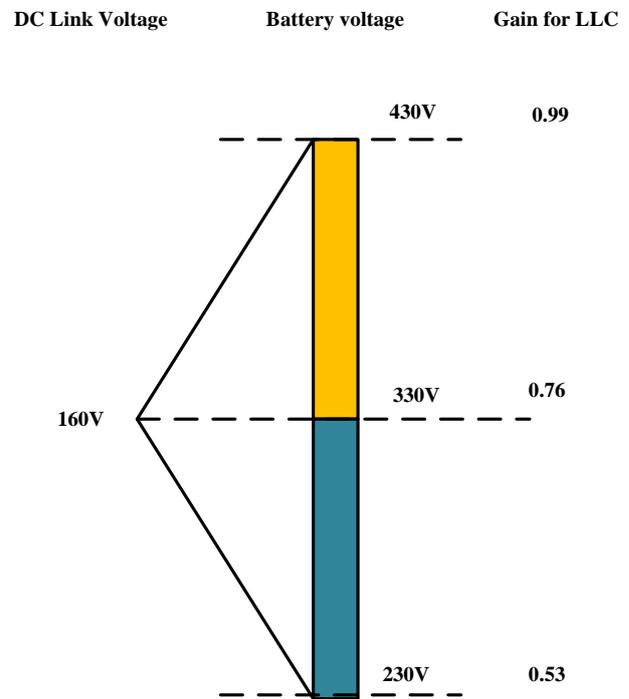

Fig. 11: Gain of LLC resonant converter.

1) Transformer Turns Ratio

Primary side minimum voltage is 160 V, maximum secondary voltage is 430 V as shown in Fig. 11 then transformer turn ratio:

$$n = \frac{v_P}{v_s} = \frac{160}{430} = 0.37. \tag{24}$$

4.2. Gain for LLC

Gain for 230 V battery is:

$$A_v = n\left[\frac{V_b}{V_{DC}}\right], \tag{25}$$

where, $V_{DC} = 160$ V.

$$A_v = 0.37 \left[\frac{230}{160} \right] = 0.53, \tag{26}$$

Similarly, for 430 V and 330 V battery, the gains are 0.99, 0.76.

Assuming, $t_{dead} = 1$ μs, $\gamma = 0.5$, $c_i = 1$ μF the desired resonant inductor L_r Eq. (22):

$$L_r = \frac{\gamma A_v t_{dead}}{2 f_s c_i} = \frac{0.5 \cdot 0.53 \cdot 1 \cdot 10^{-6}}{2 \cdot 20 \cdot 10^3 \cdot 1 \cdot 10^{-6}} = 6.62 \, \mu\text{H}. \tag{27}$$

With the increasing efficiency, the battery voltage is switched between 430–230 V, and the voltage gain is reduced. To achieve ZVS, for LLC resonant converter lower the voltage gain value used it leads to lower L_r. For example, in the Fig. 11 when the voltage gain value is 0.99, the ZVS cannot be achieved even with low value of L_r.

4.3. Battery Design

For 430 V Li-ion battery, the battery capacity has been determined by considering of motor specifications, motor power = 10 kw, Battery Voltage (VB) = 430 V.

Step 1: Current consumed by the motor:

$$P_M = V_b I_B, \tag{28}$$

$$I_b = \frac{P_M}{V_B} = 23.25 \, \text{A}. \tag{29}$$

Step 2: Watt Hour calculation:

Assuming running time is equal to 1 hr:

$$P = 10000 \cdot 1 \, watt - hr, \tag{30}$$

$$P = 10000 \, watt - hr. \tag{31}$$

Step 3: Battery capacity Calculation:

The source must have 20–30 % more than required energy:

Watt hour $= 10000 \cdot 1.2 = 12000$.

Battery capacity $= \frac{Watt\,hour}{V_B} = \frac{12000}{430}$.

Battery capacity $= 27.9070$ Ah.

4.4. Control Strategy for Battery Charging

With the current PI controller, the Bidirectional DC-DC converter is controlled to achieve CC charging for the Li-ion battery. In CV mode, the voltage PI controller regulates the Battery Voltage (V_B) for charging.

The Open Circuit Voltage (V_{oc}) is used as the battery's reference voltage at 80 % SOC. The reference current, I_{REF} for the current loop is generated from the voltage PI controller through proper gain adjustments, later it is compared with battery current, I_B. To minimize the current error by adjusting the current controller gains which keeps the desired charging current as shown in Fig. 12. This method is known as CC charging mode.
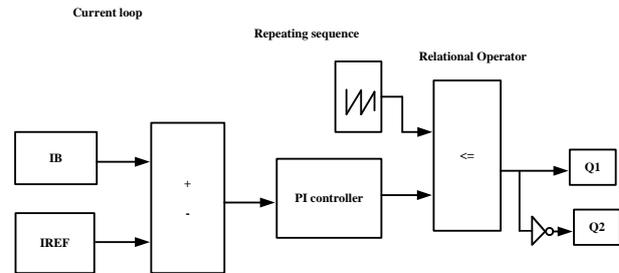

Fig. 12: Generating pulses of Bidirectional Dc-Dc Converter.

However, in CV mode, charging is obtained when the battery SOC reaches 80 %. The current PI controller becomes inactive during this time because the voltage PI controller has come out of saturation and the battery is charging to achieve full SOC.

V_B is compared with reference voltage or V_{oc} to minimize the voltage error, by adjusting the voltage controller gain to the charger as shown in Fig. 13. In CC-CV mode the battery has charged by providing of a duty cycle range. The pulses are generated for bidirectional DC-DC converter, by comparing the current PI controller with sawtooth wave switching.
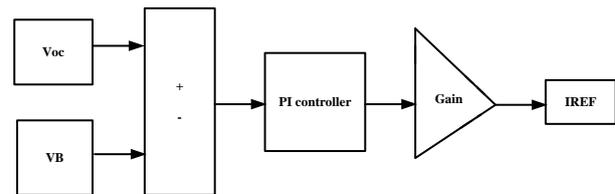

Fig. 13: EV battery current generation.

Figure 14 depicts the CC-CV algorithm's control flow chart for the bidirectional DC-DC converter for the battery.

5. Simulation Results

Detailed MATLAB/Simulink are shown to the proposed QAB converter under balancing condition. The dynamic performance of QAB converter is assessed under balancing conditions shown in Fig. 15.
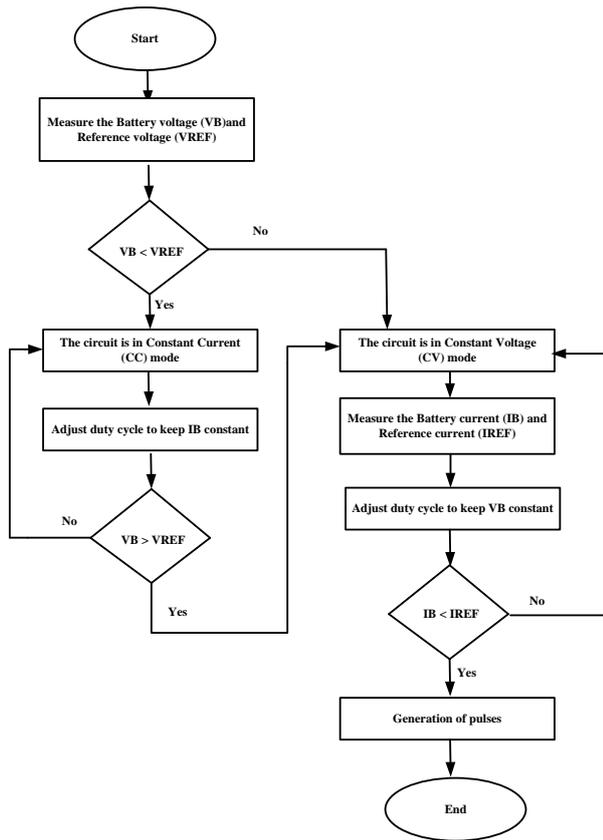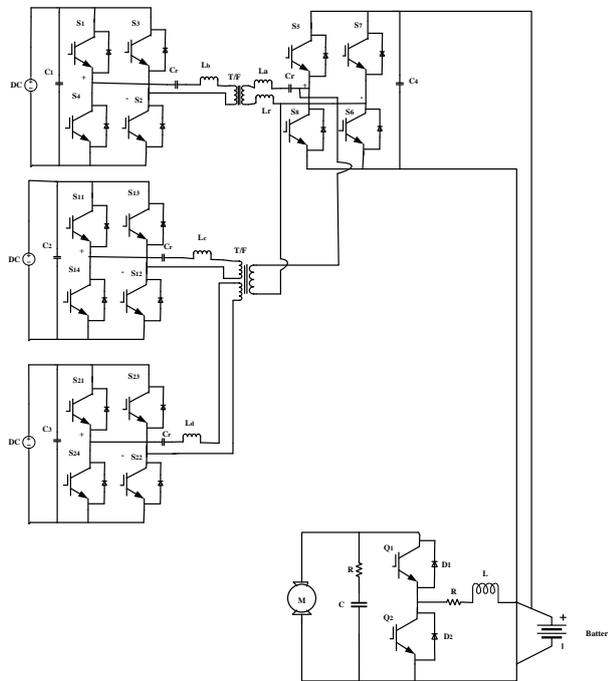
Fig. 14: Flow chart of battery in CC-CV algorithm.

Fig. 15: Proposed QAB - LLC converter with EV Battery.

5.1. Steady State Operation

QAB converter is simulated with the following specifications as presented in Tab. 3.

Tab. 3: QAB converter specification.

Symbol	Description	Value
Vin or v_M	Input voltage	480 V
LMV$_{(b,c,d)}$	Leakage inductance on MV side	373.16 µH
LLV$_{(a)}$	Leakage inductance on LV side	73.50 µH
C_r	Resonant capacitor	1.5 µF
L_r	Resonant inductor	6.62 µH
N	Turns ratio	3
f_s	Switching frequency	20 kHz

Figure 16, Fig. 17 and Fig. 18 shows the inductor current waveforms MV cell on i_{lb}, i_{Lc}, i_{Ld} and on LV cell Ila and voltage waveforms on MV side and LV side Hence, minimal inductor current stress can be achieved from the LLC resonant converter on LV side of QAB converter.
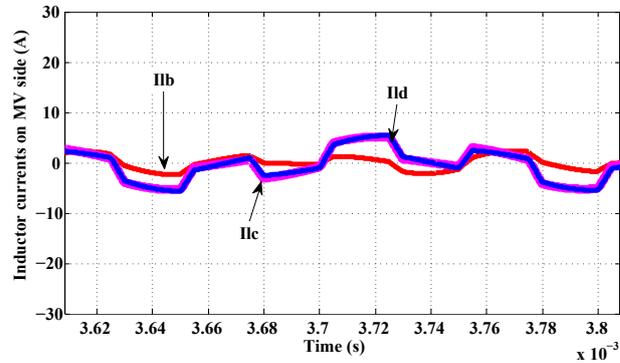

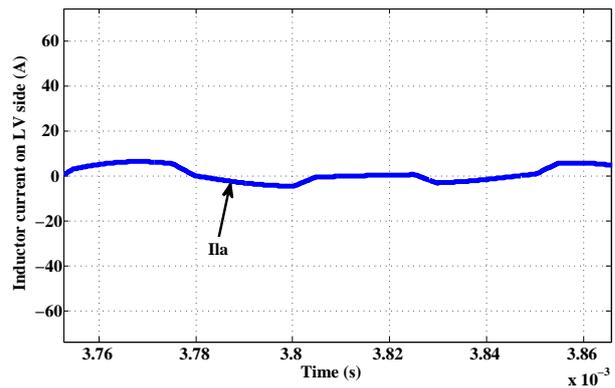**Fig. 16:** Inductor current waveforms on MV side.

Fig. 17: Inductor current waveforms on LV side.

After implementation of the proposed QAB-LLC converter, QAB-LLC fed to EV's battery with the following specifications shown in Tab. 4.

The input voltage of the QAB-LLC converter is determined depending on the voltage range of the battery for charging, and the resonant frequency (f_r) is equal to the switching frequency (f_s) to improve efficiency.
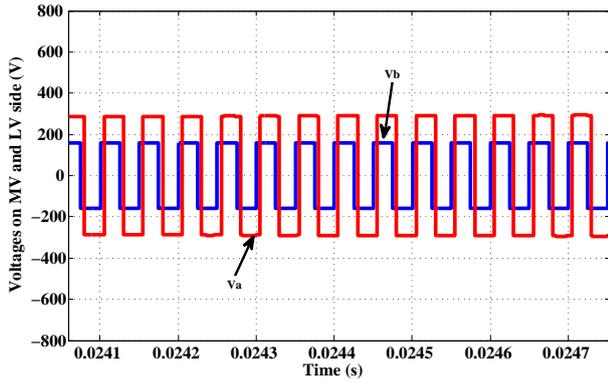
Fig. 18: Voltage on MV and LV side.

Tab. 4: Li-ion battery specifications.

Battery Voltage (V_B)	Battery capacity (Ah)	SOC (%)
430 V	27.9070	50

Hence it is, implemented with the CC-CV charging algorithm, it generates a maximum voltage of 464.7 V, 8.0245 A battery current, 50 % maximum SOC. It will generate a 97 % efficiency as shown in Fig. 19, Fig. 20 and Fig. 21 along with 27.9070 Ah battery capacity.
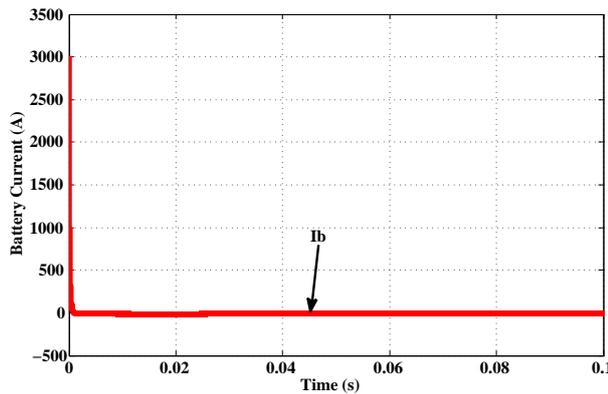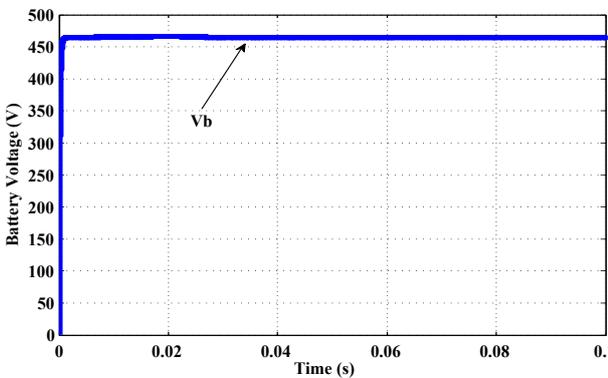

Fig. 19: Battery Voltage.

Fig. 20: Battery Current.

The proposed QAB-LLC resonant converter fed with EV battery provides small inductor current stress with
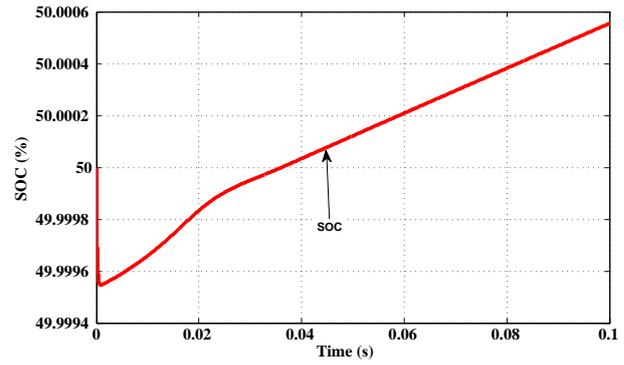

Fig. 21: Battery SOC.

respect to QAB SRC, QAB, QAB-LLC as shown in Fig. 22. Depending on resonant converter and transformer turns ratio, low amount of inductor current stress is achieved with increasing efficiency.
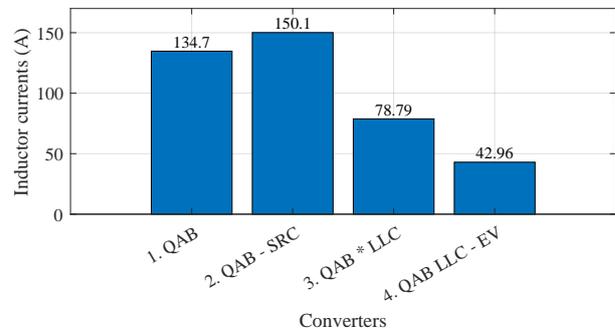

Fig. 22: Inductor current stress.

6. Conclusion

To meet the DC-DC converter's high-efficiency criteria for an energy storage system, this paper presented a detailed design, implementing a novel QAB based LLC converter. The number of circuit elements, efficiency, and complexity of various DC-DC converter-based balancing topologies were analyzed. First, The DAB has been used to provide bidirectional power flow capabilities with a 93.27 % efficiency, has presented in Tab. 5. However it will be unable to handle the load if the power level is increased. So, the review of the QAB converter concerning DAB contains a modulation scheme, soft switching characteristics, large inductor current stress on the LV side at a 95 % efficiency. Then the QAB LLC was been designed and evaluated, to determine the leakage inductance parameters which in turn minimize the inductor current stress on the LV side. In addition, this novel QAB LLC converter fed with EV battery has been verified in MATLAB/Simulink which presents 97 % efficiency achieved with 42.96 % minimum inductor current stress on LV side of QAB, 50 % maximum SOC, greater

voltage stability along with DC link voltage depending on battery parameters and efficiency comparison presented in Tab. 5.

Tab. 5: Comparison of various bidirectional DC-DC converter.

Converter	Input voltage (V)	Output voltage (V)	Efficiency (%)
DAB	110	117.9	93.27
QAB	480	456	95
Proposed: QAB LLC – EV Battery	480	464.7	97

The findings show that the proposed QAB LLC can be used in EV battery systems to achieve high efficiency while reducing inductor current stress.

Acknowledgment

Author Contributions

A.K.B. developed the theoretical concept, performed analytical calculations and MATLAB simulations. Both the authors contributed to the final version of the manuscript. J.B. supervised the total project with a good number of suggestions.

References

[1] BOULANGER, A. G., A. C. CHU, S. MAXX and D. L. WALTZ. Vehicle Electrification: Status and Issues. *Proceedings of the IEEE.* 2011, vol. 99, iss. 6, pp. 1116–1138. ISSN 1558-2256. DOI: 10.1109/JPROC.2011.2112750.

[2] SCHEWEL, L. and D. M. KAMMEN. Smart Transportation: Synergizing Electrified Vehicles and Mobile Information Systems. *Environment: Science and Policy for Sustainable Development.* 2010, vol. 52, iss. 5, pp. 24–35. ISSN 1939-9154. DOI: 10.1080/00139157.2010.507143.

[3] INOUE, S. and H. AKAGI. A Bidirectional DC–DC Converter for an Energy Storage System With Galvanic Isolation. *IEEE Transactions on Power Electronics.* 2007,

vol. 22, iss. 6, pp. 2299–2306. ISSN 0885-8993. DOI: 10.1109/TPEL.2007.909248.

[4] DAS, P., B. LAAN, S. A. MOUSAVI and G. MOSCHOPOULOS. A Nonisolated Bidirectional ZVS-PWM Active Clamped DC–DC Converter. *IEEE Transactions on Power Electronics.* 2009, vol. 24, iss. 2, pp. 553–558. ISSN 1941-0107. DOI: 10.1109/TPEL.2008.2006897.

[5] PAHLEVANINEZHAD, M., P. DAS, J. DROBNIK, P. K. JAIN and A. BAKHSHAI. A Novel ZVZCS Full-Bridge DC/DC Converter Used for Electric Vehicles. *IEEE Transactions on Power Electronics.* 2012, vol. 27, iss. 6, pp. 2752–2769. ISSN 1941-0107. DOI: 10.1109/TPEL.2011.2178103.

[6] PAHLEVANINEZHAD, M., J. DROBNIK, P. K. JAIN and A. BAKHSHAI. A Load Adaptive Control Approach for a Zero-Voltage-Switching DC/DC Converter Used for Electric Vehicles. *IEEE Transactions on Industrial Electronics.* 2012, vol. 59, iss. 2, pp. 920–933. ISSN 1557-9948. DOI: 10.1109/TIE.2011.2161063.

[7] JIANG, T., J. ZHANG, X. WU, K. SHENG and Y. WANG. A Bidirectional LLC Resonant Converter With Automatic Forward and Backward Mode Transition. *IEEE Transactions on Power Electronics.* 2015, vol. 30, iss. 2, pp. 757–770. ISSN 1941-0107. DOI: 10.1109/TPEL.2014.2307329.

[8] JIANG, T., J. ZHANG, X. WU, K. SHENG and Y. WANG. A Bidirectional Three-Level LLC Resonant Converter With PWAM Control. *IEEE Transactions on Power Electronics.* 2016, vol. 31, iss. 3, pp. 2213–2225. ISSN 1941-0107. DOI: 10.1109/TPEL.2015.2438072.

[9] DENG, J., S. LI, S. HU, C. C. MI and R. MA. Design Methodology of LLC Resonant Converters for Electric Vehicle Battery Chargers. *IEEE Transactions on Vehicular Technology.* 2014, vol. 63, iss. 4, pp. 1581–1592. ISSN 1939-9359. DOI: 10.1109/TVT.2013.2287379.

[10] SHAHZAD, M. I., S. IQBAL and S. TAIB. Interleaved LLC Converter With Cascaded Voltage-Doubler Rectifiers for Deeply Depleted PEV Battery Charging. *IEEE Transactions on Transportation Electrification.* 2018, vol. 4, iss. 1, pp. 89–98. ISSN 2332-7782. DOI: 10.1109/TTE.2017.2753407.

[11] TA, L. A. D., N. D. DAO and D.-C. LEE. High-Efficiency Hybrid LLC Resonant Converter for On-Board Chargers of Plug-In Electric Vehicles. *IEEE Transactions on Power Electronics.* 2020,

vol. 35, iss. 8, pp. 8324–8334. ISSN 1941-0107. DOI: 10.1109/TPEL.2020.2968084.

[12] ZHAO, B., Q. SONG, W. LIU and Y. SUN. Overview of Dual-Active-Bridge Isolated Bidirectional DC–DC Converter for High-Frequency-Link Power-Conversion System. *IEEE Transactions on Power Electronics*. 2014, vol. 29, iss. 8, pp. 4091–4106. ISSN 1941-0107. DOI: 10.1109/TPEL.2013.2289913.

[13] RODRIGUEZ, A., A. VAZQUEZ, D. G. LAMAR, M. M. HERNANDO and J. SEBASTIAN. Different Purpose Design Strategies and Techniques to Improve the Performance of a Dual Active Bridge With Phase-Shift Control. *IEEE Transactions on Power Electronics*. 2015, vol. 30, iss. 2, pp. 790–804. ISSN 1941-0107. DOI: 10.1109/TPEL.2014.2309853.

[14] XUAN, Y., X. YANG, W. CHEN, T. LIU and X. HAO. A Three-Level Dual-Active-Bridge Converter With Blocking Capacitors for Bidirectional Electric Vehicle Charger. *IEEE Access*. 2019, vol. 7, iss. 1, pp. 173838–173847. ISSN 2169-3536. DOI: 10.1109/ACCESS.2019.2957022.

[15] GILL, L., T. IKARI, T. KAI, B. LI, K. NGO and D. DONG. Medium Voltage Dual Active Bridge Using 3.3 kV SiC MOSFETs for EV Charging Application. In: *2019 IEEE Energy Conversion Congress and Exposition (ECCE)*. Baltimore: IEEE, 2019, pp. 1237–1244. ISBN 978-1-72810-395-2. DOI: 10.1109/ECCE.2019.8912874.

[16] YAQOOB, M., K. H. LOO and Y. M. LAI. A Four-Degrees-of-Freedom Modulation Strategy for Dual-Active-Bridge Series-Resonant Converter Designed for Total Loss Minimization. *IEEE Transactions on Power Electronics*. 2019, vol. 34, iss. 2, pp. 1065–1081. ISSN 1941-0107. DOI: 10.1109/TPEL.2018.2865969.

[17] WEN, H., W. XIAO and B. SU. Nonactive Power Loss Minimization in a Bidirectional Isolated DC–DC Converter for Distributed Power Systems. *IEEE Transactions on Industrial Electronics*. 2014, vol. 61, iss. 12, pp. 6822–6831. ISSN 1557-9948. DOI: 10.1109/TIE.2014.2316229.

[18] ZHAO, B., Q. YU and W. SUN. Extended-Phase-Shift Control of Isolated Bidirectional DC–DC Converter for Power Distribution in Microgrid. *IEEE Transactions on Power Electronics*. 2012, vol. 27, iss. 11, pp. 4667–4680. ISSN 1941-0107. DOI: 10.1109/TPEL.2011.2180928.

[19] HUANG, J., Y. WANG, Z. LI and W. LEI. Unified Triple-Phase-Shift Control to Minimize Current Stress and Achieve Full Soft-Switching of Isolated Bidirectional DC–DC Converter. *IEEE Transactions on Industrial Electronics*. 2016, vol. 63, iss. 7, pp. 4169–4179. ISSN 1557-9948. DOI: 10.1109/TIE.2016.2543182.

[20] TAYLOR, A., G. LIU, H. BAI, A. BROWN, P. M. JOHNSON and M. MCAMMOND. Multiple-Phase-Shift Control for a Dual Active Bridge to Secure Zero-Voltage Switching and Enhance Light-Load Performance. *IEEE Transactions on Power Electronics*. 2018, vol. 33, iss. 6, pp. 4584–4588. ISSN 1941-0107. DOI: 10.1109/TPEL.2017.2769638.

[21] LI, B., Q. LI, F. C. LEE, Z. LIU and Y. YANG. A High-Efficiency High-Density Wide-Bandgap Device-Based Bidirectional On-Board Charger. *IEEE Journal of Emerging and Selected Topics in Power Electronics*. 2018, vol. 6, iss. 3, pp. 1627–1636. ISSN 2168-6785. DOI: 10.1109/JESTPE.2018.2845846.

[22] MENDOLA, M. L., M. DI BENEDETTO, A. LIDOZZI, L. SOLERO and S. BIFARETTI. Four-Port Bidirectional Dual Active Bridge Converter for EVs Fast Charging. In: *2019 IEEE Energy Conversion Congress and Exposition (ECCE)*. Baltimore: IEEE, 2019, pp. 1341–1347. ISBN 978-1-72810-395-2. DOI: 10.1109/ECCE.2019.8912252.

[23] WEN, H., J. LI, H. SHI, Y. HU and Y. YANG. Fault Diagnosis and Tolerant Control of Dual-Active-Bridge Converter With Triple-Phase Shift Control for Bidirectional EV Charging Systems. *IEEE Transactions on Transportation Electrification*. 2021, vol. 7, iss. 1, pp. 287–303. ISSN 2372-2088. DOI: 10.1109/TTE.2020.3045673.

[24] COSTA, L. F., F. HOFFMANN, G. BUTICCHI and M. LISERRE. Comparative Analysis of Multiple Active Bridge Converters Configurations in Modular Smart Transformer. *IEEE Transactions on Industrial Electronics*. 2019, vol. 66, iss. 1, pp. 191–202. ISSN 1557-9948. DOI: 10.1109/TIE.2018.2818658.

[25] NAIR, A. C., M. J. VISHAL and B. G. FERNANDES. A Quad Active Bridge Based on-Board Power Electronic Interface for an Electric Vehicle. In: *2018 IEEE Energy Conversion Congress and Exposition (ECCE)*. Portland: IEEE, 2018, pp. 5941–5947. ISBN 978-1-4799-7312-5. DOI: 10.1109/ECCE.2018.8557650.

[26] FRUTOS, P., F. BRIZ, A. SANCHEZ and J. M. GUERRERO. Quad-Active-Bridge as the basic cell of a MMC Based SST for DER and DESS Integration. In: *2019 IEEE*

28th International Symposium on Industrial Electronics (ISIE). Vancouver: IEEE, 2019, pp. 2349–2355. ISBN 978-1-72813-666-0. DOI: 10.1109/ISIE.2019.8781463.

[27] NAIR, A. C. and B. G. FERNANDES. A Solid State Transformer based Fast Charging Station for all Categories of Electric Vehicles. In: *IECON 2018 - 44th Annual Conference of the IEEE Industrial Electronics Society*. Washington: IEEE, 2018, pp. 1989–1994. ISBN 978-1-5090-6684-1. DOI: 10.1109/IECON.2018.8592739.

[28] NASEEM, N. and H. CHA. Quad-Active-Bridge Converter With Current Balancing Coupled Inductor for SST Application. *IEEE Transactions on Power Electronics*. 2021, vol. 36, iss. 11, pp. 12528–12539. ISSN 1941-0107. DOI: 10.1109/TPEL.2021.3076460.

[29] BANDYOPADHYAY, S., P. PURGAT, Z. QIN and P. BAUER. A Multiactive Bridge Converter With Inherently Decoupled Power Flows. *IEEE Transactions on Power Electronics*. 2021, vol. 36, iss. 2, pp. 2231–2245. ISSN 1941-0107. DOI: 10.1109/TPEL.2020.3006266.

[30] SWAMINATHAN, N. and Y. CAO. An Overview of High-Conversion High-Voltage DC–DC Converters for Electrified Aviation Power Distribution System. *IEEE Transactions on Transportation Electrification*. 2020, vol. 6, iss. 4, pp. 1740–1754. ISSN 2372-2088. DOI: 10.1109/TTE.2020.3009152.

[31] HANNAN, M. A., P. J. KER, M. S. H. LIPU, Z. H. CHOI, M. S. A. RAHMAN, K. M. MUTTAQI and F. BLAABJERG. State of the Art of Solid-State Transformers: Advanced Topologies, Implementation Issues, Recent Progress and Improvements. *IEEE Access*. 2020, vol. 8, iss. 1, pp. 19113–19132. ISSN 2169-3536. DOI: 10.1109/ACCESS.2020.2967345.

[32] COSTA, L. F., G. BUTICCHI and M. LISERRE. Quadruple Active Bridge DC-DC converter as the basic cell of a modular Smart Transformer. In: *2016 IEEE Applied Power Electronics Conference and Exposition (APEC)*. Long Beach: IEEE, 2016, pp. 2449–2456. ISBN 978-1-4673-9550-2. DOI: 10.1109/APEC.2016.7468209.

[33] COSTA, L. F., G. BUTICCHI and M. LISERRE. Optimum Design of a Multiple-Active-Bridge DC–DC Converter for Smart Transformer. *IEEE Transactions on Power Electronics*. 2018, vol. 33, iss. 12, pp. 10112–10121. ISSN 1941-0107. DOI: 10.1109/TPEL.2018.2799680.

[34] COSTA, L. F., G. BUTICCHI and M. LISERRE. Quad-Active-Bridge DC–DC Converter as Cross-Link for Medium-Voltage Modular Inverters. *IEEE Transactions on Industry Applications*. 2017, vol. 53, iss. 2, pp. 1243–1253. ISSN 1939-9367. DOI: 10.1109/TIA.2016.2633539.

[35] SHE, X., A. Q. HUANG and R. BURGOS. Review of Solid-State Transformer Technologies and Their Application in Power Distribution Systems. *IEEE Journal of Emerging and Selected Topics in Power Electronics*. 2013, vol. 1, iss. 3, pp. 186–198. ISSN 2168-6785. DOI: 10.1109/JESTPE.2013.2277917.

[36] PANY, P., R. SINGH and R. TRIPATHI. Bidirectional DC-DC converter fed drive for electric vehicle system. *International Journal of Engineering, Science and Technology*. 2011, vol. 3, iss. 3, pp. 101–110. ISSN 2141-2820. DOI: 10.4314/ijest.v3i3.68426.

About Authors

Anil Kumar BOYA is currently pursuing his Ph.D. degree from Koneru Lakshmaiah Educational Foundation (Deemed to be University), Greenfields, 522502 Vaddeswaram, Andhra Pradesh, India. He received his M.Tech. from Challa Malla Reddy College of Engineering and Technology, Hyderabad, Telangana, India and B.Tech from Kandula Sreenivasa Reddy Memorial College of Engineering, Kadapa, Andhra Pradesh, India. His areas of interest are Power Electronics, Electric Vehicles.

Batchalakura JYOTHI is presently working as an Assoc. Professor in Electrical and Electronics Engineering Department of Koneru Lakshmaiah Educational Foundation (Deemed to be University), Vaddeswaram, Andhra Pradesh, India. She received her Ph.D. degree from Acharya Nagarjuna university, Guntur, Andhra Pradesh, India, M.Tech. from JNTU Hyderabad and B.Tech. from S.K. University, Anathapur. She is a Life Member of ISTE. She is 17 years of experience in teaching and has published papers in indexed Scopus & SCI journals, presented papers at prestigious INDICON & TENCON IEEE conferences. Published three commercial patents. Her areas of interest are Power Electronics, Electrical vehicles, Smart Grids, Micro Grids and Cyber Security.

Appendix A

The power of QAB converter with respect to turns ratio is given as:

$$P_{QAB} = \frac{Rated\,power}{n} = \frac{1\,\text{MW}}{3} = 333\,\text{kW}. \quad (32)$$

The MV DC link is:

$$v_M = \frac{v_{MVDC}}{n} = \frac{480}{3} = 160\,\text{V}. \quad (33)$$

The LV DC link is:

$$v_L = v_{LVDC} = 430\,\text{V}. \quad (34)$$

The value of inductor L_{MV} is calculated from the Eq. (18):

$$L = \frac{3D_1^2 \left(v_M - nv_L\right)\left(nv_L\right)^2}{4f_s P_b v_M}, \quad v_M > v_L. \quad (35)$$

The value of inductor on MV side is negative but it should be neglected because depending on number of turns ratio regarding with MV and LV side. Depending on same value of leakage inductance on MV side, the QAB LLC converter should get the trapezoidal inductor current waveforms and also due to incomplete construction of transformer the MV inductor should affected in order to reduce this effect additional inductor should be added on MV side which should be greater than the LV side inductor.

The duty cycle, turns ratio and P_b or P_{QAB} are 0.5, 3 and 333 kW are substitute in above equation:

$$L = \frac{3 \cdot (0.5)^2 \cdot [160 - (3 \cdot 430)] \cdot (3 \cdot 430)^2}{4 \cdot 20 \cdot 10^3 \cdot 333 \cdot 10^3 \cdot 160}, \quad (36)$$

$$L = 330.8\,\mu\text{H}. \quad (37)$$

The MV side inductors are $L_b = L_c = L_d = L(b,c,d) = 330.8\,\mu\text{H}$.

The turns ratio for the LV side inductor must be considered.

Appendix B Calculation of L_{MV} and L_{LV}

$$L_a = \frac{L}{n^2} = \frac{330.8}{9} = 36.75\,\mu\text{H}. \quad (38)$$

The required leakage inductance on LV side is calculated by the Eq. (7):

$$L_{equ} = L_a + \frac{L_b + L_c + L_d}{3n^2}, \quad (39)$$

$$L_{equ} = 36.75 + \frac{330.8 + 330.8 + 330.8}{27}, \quad (40)$$

$$L_{equ} = 73.50\,\mu\text{H}. \quad (41)$$

The LV side inductor is $L_{equ} = L_{aLV} = 73.50$ μH.

The leakage inductance of the MV side is affected due to the incomplete construction of the transformer. On the MV side, an external inductor should be installed to reduce this problem and it's specifications listed in Tab. 6.

Tab. 6: Transformer specifications.

Leakage Inductance	$L_{a'LV}$	$L_{b'MV}$	$L_{c'MV}$	$L_{d'MV}$
Values	40.7 μH	16.5 μH	13.5 μH	15 μH

The external inductor can be calculated by considering the specifications presented in Tab. 6 and used by the Eq. (7).

$$L_{ext} = L_{a'LV} + \frac{L_{b'MV} + L_{c'MV} + L_{d'MV}}{3n^2}, \quad (42)$$

$$L_{ext} = 40.7 + \frac{16.5 + 13.5 + 15}{3 \cdot 9}, \quad (43)$$

$$L_{ext} = 42.36\,\mu\text{H}, \quad (44)$$

$$L_{(b,c,d)MV} = L_{(b,c,d)} + L_{ext}, \quad (45)$$

$$L_{(b,c,d)MV} = 330.8 + 42.36 = 373.16\,\mu\text{H}. \quad (46)$$